Validation of the CMS Track-Finder Trigger in a muon beam test

Nicholas S. Park
University of Florida
Gainesville, Florida

Darin Acosta
University of Florida
Gainesville, Florida

Abstract

Following the CMS Cathode Strip Chamber Beam Test of Summer 2004, experimental validation of the performance of CMS Track-Finder Trigger is necessary. This study focuses on the analysis of the beam profile, ϕ distribution fits, the beam scattering due to iron blocks in the muon beam path, and the comparison of the Track-Finder Trigger hardware output to a software simulation. Employing statistical distribution comparisons, it was found that iron blocks in a 100 GeV muon beam resulted in minimal beam scattering, an ideal condition for the CMS detector. In addition, beam profile analysis and the statistical fitting of ϕ distribution plots was optimized for the creation of Lookup Tables (LUT), an integral part of the Track-Finder system, specific to the Beam Test chamber layout. Most importantly, the Sector Processor Core Logic of the Track-Finder Trigger was verified to be in perfect agreement with the software simulation, validating its ability to reconstruct muon tracks.

I. INTRODUCTION

A. CERN and the LHC

Scheduled for completion in 2007, the Large Hadron Collider (LHC) will be the world's most powerful particle accelerator to date. The LHC is the latest step by the European Organization for Nuclear Research (CERN) to probe deeper into matter than ever before. With a radius of 2.67 miles (4.30 km) and a circumference of 16.77 miles (27 km), the LHC accelerator ring will collide a pair of proton beams at a combined energy of 14 TeV with a luminosity of $10^{34}cm^{-2}s^{-1}$. This is a significant leap beyond the 2 TeV collision energies of current highest-energy particle accelerator, the Tevatron at Fermi National Accelerator Laboratory. Construction of the LHC makes use of CERN's previous underground accelerator tunnel, the Large Electron-Positron Collider (LEP), but with extensive modification for the increase in collision energies as well accommodation for two main detectors. [1]

B. Physics at the LHC

The near ten-fold collision energy increase over the Tevatron will allow the LHC to peer further into the primary structure of matter than ever before. One of the most confounding questions in physics centers around the explanation of particle masses. The Standard Model attempts to answer this question through the Higgs mechanism: a field, called the Higgs field, permeates the entire universe and with which a particle's interaction causes it to have mass. The particle associated with the Higgs mechanism is the Higgs boson. Current collider energy and luminosity, however, are unable to reach the levels necessary for the creation and detection of a Higgs boson. A clean method to detect the Higgs boson would be through its decay into two Z bosons, where each Z further decays into two muons. The discovery of the four final-state muons of the Higgs boson decay would be a direct confirmation of the existence of the Higgs

boson, allowing the calculation of the invariant mass of the Higgs. If the Higgs boson exists, the LHC should be able to detect it. [1]

The LHC should also be able to discover supersymmetric particles, if they exist. Supersymmetry (SUSY) is a theory that avoids fine-tuning certain parameters in current particle theories by introducing partners to all the known particles with opposite spin statistics, such as what fermions would be to bosons. Such a postulate also allows for the unification of the forces, including gravity, if string theory is correct.

C. The Compact Muon Solenoid

For the LHC, two primary detectors are under development: ATLAS and the Compact Muon Solenoid, CMS (see Fig. 1). The CMS Detector is 21.60 m in length with a 14.6 m diameter that incorporates a superconducting solenoid with muon detectors, calorimeters, and a silicon tracker. The CMS solenoid will be the largest solenoid ever built and will supply a maximum magnetic field of 4 Tesla. The CMS muon detectors are divided into two main sections: the CMS barrel muon detector and the CMS Endcap Muon (EMU) system. The barrel muon detector is composed of Drift Tubes (DT) while the EMU system is composed of Cathode Strip Chambers (CSC), with Resistive Parallel Plate Chambers (RPC) in both the barrel and endcap muon detectors. Each endcap is subdivided into four discs, called stations, each denoted by ME*n*, where *n* refers to the station number (1-4). Structurally, each station is further divided into concentric rings containing one of seven sizes of CSCs. Functionally, each station is divided into sectors, like a pie, for purposes of reconstructing muons in the Level-1 Trigger system: 60º slices for ME2,

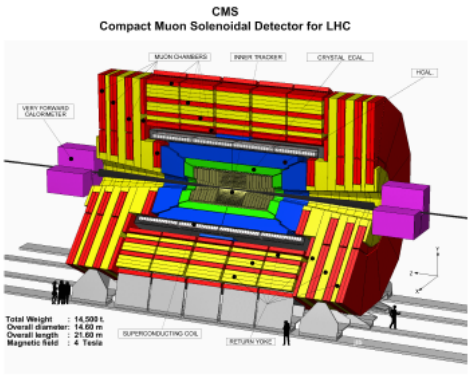

FIGURE 1: 3-D rendering of the CMS Detector

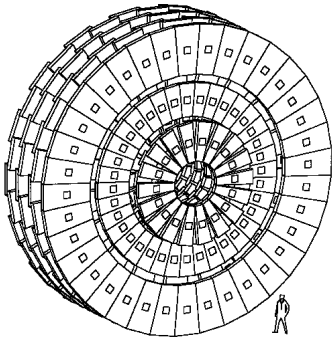

FIGURE 2: Endcap muon chamber layout

ME3, and ME4 and 30º slices for ME1, the innermost endcap station. All 540 of the CSCs that make up the endcap are arranged and layered such that there is almost 100% coverage over the endcap region (see Fig. 2).

Each Cathode Strip Chamber is of a trapezoidal shape and contains six planes of honeycomb panel, each topped with etched copper strips that run radially in the overall geometry of the endcap system with a final honeycomb panel on top. In addition to the copper strips, each plane also has a set of wires stretched across the width of the chamber that are grouped for data readout and to which a high voltage has been applied. Between the layered planes is an open space called the gas gap, through which a mixture of CO_2, Ar, and CF_4 gas is constantly being pumped. [1]

The CMS detector system will produce, at its most basic levels, monumental volumes of data each second. This is on the order of 100 Terabytes each second or, for a common comparison, approximately 10,000 Encyclopedia Britannica's worth of data each second. CMS designates the responsibility of reducing this volume of data to its Trigger and Data Acquisition System, TriDAS, which selects only a small fraction of all collisions for further analysis. Two parts of the TriDAS system are the CSC Local Trigger and the CSC Track-Finder, collectively grouped as part of the Level-1 Trigger System.

D. CSC Local Trigger System

With a high voltage applied to the wires in the CSC, when a particle such as a muon passes through one of the CSC planes, a charge is induced across several of the strips and wires of that plane (see Fig. 3). Here, the copper strips act as the

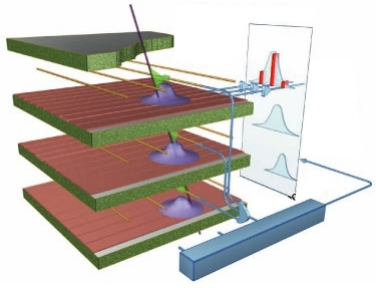

FIGURE 3: Rendition of the charge buildup across several strips in different CSC layers

cathode while the wires act as the anode. Each CSC contains two sets of electronics responsible for amplifying the electric signal caused by the induced charges: a Cathode Front End Board (CFEB) and an Anode Front End Board (AFEB).

The output of the AFEB goes to the Anode Local Charged Track (ALCT)-finding board, which resides on the CSC. The ALCT board takes a set of wire group hits from the AFEB and performs pattern recognition to identify charged tracks across the 6 planes. Up to two ALCTs per chamber are reported. These ALCTs are also assigned a specific bunch crossing number, the 25 ns timing blocks used in CMS data-taking.

The output of the CFEB and the output of the ALCT board then go to a rack-mounted hardware crate called the Peripheral Crate. In the Peripheral Crate, the CFEB data are first processed by the Cathode LCT-finding circuit to form a Cathode LCT (CLCT) from the hit-patterns on the CSC strips. Then, the ALCT and CLCT are sent to the Trigger Motherboard (TMB), which combines the ALCT and CLCT of a specific bunch crossing as a Correlated LCT. In addition, a quality value is assigned to each Correlated LCT, determined by the hit patterns of the ALCT and CLCT and the number of CSC layers upon which the LCT was found. The CLCT-finding circuit actually resides on the same hardware board as the TMB. Of all the Correlated LCTs created by the TMB, the best two in quality are then sent on to the Muon Port Card. [2]

E. Muon Port Card

Each Muon Port Card (MPC) receives up to two Correlated LCTs from all TMBs in one sector of one endcap muon station. Performing a simple but necessary task, the MPC selects the three most interesting Correlated LCTs and sends them via optical fiber links to the CSC Track-Finder System for further processing. [2]

II. CSC Track-Finder System

A. Overall Design and Purpose

The CSC Track-Finder System is the next step in the overall Level-1 Trigger system. It further narrows the selection of "interesting" events and is the device responsible for reconstructing the trajectories of muons from the Correlated LCTs outputted by the MPC. With the muon tracks reconstructed, the Track-Finder System is able to measure the transverse momentum (p_T), pseudo-rapidity (η), and the azimuthal angle (ϕ) of each muon. To have an acceptable level of rate reduction, a p_T resolution of 25% is necessary. After the reduction in event rates performed by the Track-Finder System, the Level-1 muons are sent to the Global Muon Trigger (GMT). [2]

B. CSC Track-Finder Architecture

1. Sector Receiver

At the receiving end of the MPC's optical links is the Track-Finder's Sector Receiver (SR), accepting the information of three muons as Correlated LCTs. Specifically, there is one SR for each MPC, with a total of 5 SRs on each Track-Finder board; i.e., two SRs for the two MPCs of ME1 and one SR for each of MPC from ME2, ME3, and ME4.

After digitizing the muon data from the optical links, the SR's Front FPGAs store the incoming data in a memory buffer. An important tool for diagnostics and testing, the Front FPGAs are able to insert dummy data into the Sector Processor, simulating the arrival of data from the MPCs. The data in the Front FPGA contains the wire group, pattern number, quality, strip ID, left/right bend, bunch crossing, and CSC ID. The strip ID is actually measured in half-strip units, as the CLCT-finding board on the TMB employs comparator bits to calculate which half of the strip the muon passed through. Sometimes a muon will cross a CSC at such a shallow

angle that a di-strip pattern, a grouping of four half-strips, must be used to find a LCT. In addition, as the chamber layout for each station is staggered with overlapping CSCs to maintain a near-complete coverage area, the Front FPGA assigns a front/rear value to each stored LCT.

The next step in the SR is the implementation of Lookup Tables (LUTs) to transform the Correlated LCT data in the Front FPGAs into data that is globally applicable to the entire CMS system. The LUTs function such that the input parameters from the LCTs in the Front FPGAs are combined to form an address in the LUT unique to those parameters. At this address lies the pre-calculated data corresponding to the given input parameters. The final output is then parsed into the designated output parameters.

To construct the full set of global coordinates for a track segment in the CMS detector, three separate LUTs are employed. First in this process, the Local Phi LUT is used to compute the local (with respect to the specific CSC) azimuth coordinate (ϕ_{local}) and the local ϕ bend angle ($\phi_{b,local}$) from the strip ID, CLCT pattern, quality, and left/right bend data in the Front FPGA. Taking the local ϕ bend angle ($\phi_{b,local}$) and the local azimuth coordinate (ϕ_{local}) from the Local Phi LUT output, the CSC ID, and the wire group ID as input to the Global Eta LUT, the global pseudo-rapidity (η) and the global ϕ bend angle (ϕ_b) are computed and outputted. Finally, the global azimuth coordinate (ϕ) is found in the Global Phi LUT, through the input of the local azimuth coordinate (ϕ_{local}), the CSC ID, and the wire group ID. [2]

2. Sector Processor

From the track segment output of the Sector Receivers, complete muon track are then reconstructed by the Sector Processor (SP). To reconstruct tracks, the SP takes a track segment and extrapolates it to another station and compares the track segments on that station with the extrapolated track segment. If there is a match between the extrapolated track segment and an

actual track segment, a track created from two segments is formed. This extrapolation and comparison process occurs for each track segment. Before any tracks can be outputted, the tracks are assembled to eliminate any redundancy; i.e., any tracks that are sub-tracks of a larger track across more chambers. A minimum of two track segments is required to form a trigger. See Fig. 4 for a representation of the reconstruction of a muon track from a set of track segments.

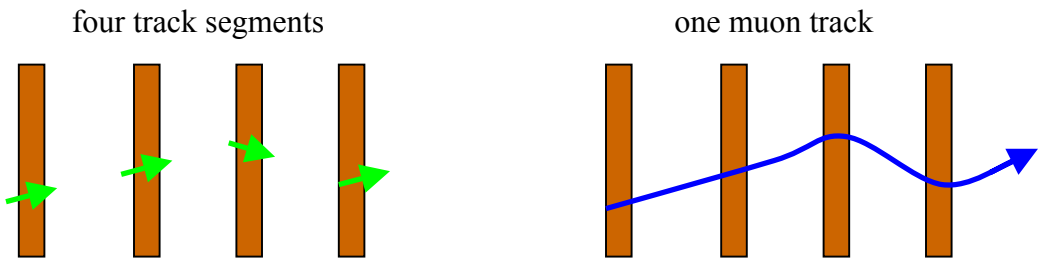

FIGURE 4: A representation of how individual track segments on different CSCs are reconstructed by the Sector Processor to form a muon track

In addition to reconstruction muon tracks, the SP also calculates the transverse momentum (p_T) for each track. This calculation is performed by another LUT, the PT LUT, which, to construct the address, takes the sign, track mode, η, and two $\Delta\phi$ values, a difference between the ϕ coordinates of two chambers. Finally, before being sent to the Muon Sorter, each track is assigned a rank, a combination of the transverse momentum (p_T) and the track quality. [2]

3. Sector Processor 2002 Prototype

The design and fabrication of the Sector Processor 2002 Prototype has been a vast improvement over the previous prototype generation, the SP2000. While originally designed as separate boards, the SP2002 Prototype allows a total of five SR boards and an updated version of the SP2000 board to be condensed onto a single board. The updated SP2002board is an intricately complex design, constructed from of 16 layers and a floating mezzanine card containing the SP Core Logic that is plugged in to the top of the SP2002 board. This update of

the SR/SP boards and logic has not only helped to reduce the number of required boards, but has significantly reduced the latency of the SR and SP logic processes by 14 bunch crossings, or 350 ns.

C. LCTs, Track Stubs, and Tracks

With such similar names, it helps to clarify the differences between the LCTs, the Track Stubs, and the Tracks, especially as there is a logical progression from one to the next. The first step in this progression, a Local Charged Track (LCT) is created from a recognized pattern of either the half-strip (or di-strip) layers or the wire group layers found in a CSC. Independent LCTs are created by the CFEB (strips) and AFEB (wire groups), which are then combined as a Correlated LCT by the TMB. Next, Track Stubs are generated from the Correlated LCTs through the LUTs on the SR board. These Track Stubs contain the global η and ϕ coordinates and are further designated by station. The final muon tracks are reconstructed by the SP through existing Track Stubs and their extrapolated tracks.

D. Muon Sorter

In the entire CMS detector, a total of 12 SPs will be required for both endcaps and the DT/CSC overlap regions. Although each SP outputs three muons, only the four best muons by rank are to be reported to the Global Muon Trigger (GMT). Thus, at each bunch crossing, of the 36 available muons, the Muon Sorter is to send the four highest-ranked muons in order of decreasing rank to the GMT. [2]

III. CMS Summer 2004 Test Beam

CMS is an international collaboration employing technology and specifically developing hardware for the CMS experiment. As much of this hardware is still under development, extensive prototype testing is required to ensure that the final CMS experiment employs

hardware and software that is as error-free as possible. Furthermore, nearly all the subsystems must interface together to form the entirety of the Level-1 Trigger and TriDAS systems. Regular testing is essential to the creation of a working system.

A. Test Beam Setup

Initially, the test beam had a chamber layout of four CSCs (ME1/1, ME1/2, ME2/2, and ME3/2) all facing parallel to each other with the muon beam normal to their surface. Such a layout can be seen in Fig. 5. For most of the data-taking runs, however, the ME2/2 and ME3/2 chambers were rotated 33.7º counterclockwise (as viewed from above; see also Fig. 9). In addition to the aforementioned rotation, a few runs had ME3/2 was rotated to face 22.5º upward. As seen in Fig. 4, two sets of iron blocks were available to be placed either before ME1/1 or between ME1/2 and ME2/2, although they were not always used. As will be addressed later, the iron blocks served to allow the testing of muon beam scattering.

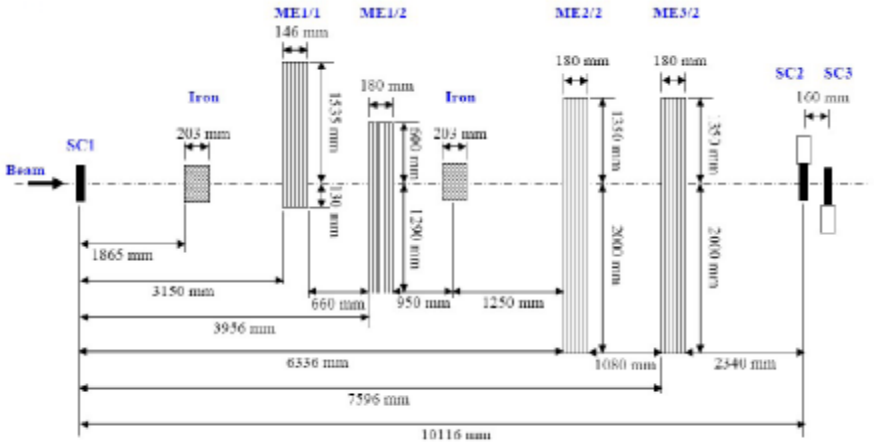

FIGURE 5: The original CSC layout at the Test Beam

In addition to varying the use of iron blocks, the Test Beam utilized two separate beam types, a muon beam and a pion beam. Both types were used to compare the differences in beam profile and trigger intensity and the effects therein.

B. Data Readout and the Data Acquisition System

For the CSCs, the data in the SR memory can be read out through two different methods as part of the Data Acquisition (DAQ) system. Through the VME interface, a hardware electronics standard for crates and boards, the TF data can be directly read from the SR board. In addition, the SP2002 board is designed with VME-readable registers for diagnostics and error logging. These error logs store the bunch crossing number and error type for any errors found.

Alternatively, the SRs of the SP2002 board can transmit data via optical link to the Front-End Driver (FED). The FED crate contains the Detector Dependant Unit (DDU), which buffers, formats, and sends the data from the SR to the Data Concentration Card (DCC), which then merges DDU data and sends it to the central DAQ system.

For the purposes of this analysis, all beam test data was read directly from the Track-Finder through its VME interface.

The DAQ system is controlled through a Graphical User Interface (GUI) that acts as a unified run control. Called the EMU Commander, the GUI controls the DAQ system through a messaging framework created specifically for CMS: XDAQ, a distributed DAQ framework. Underlying the XDAQ framework, Simple Object Access Protocol (SOAP) and Intelligent Input/Output (I_2O) messaging standards allow the full control of XDAQ-based software across networks through command and data transfer.

C. Trigger Source

Labeled as SC1, SC2, and SC3 in Fig. 5, three scintillators were used as one of two triggering methods in the test beam. The scintillators act as a basic Level-1 Accept (L1A) Trigger by detecting the presence of a muon passing through them and then sending the L1A signal to start data readout. For nearly all the later runs and, subsequently, the majority of runs used in this analysis, the Track-Finder itself was set up to self-trigger upon valid reconstruction

of a muon. In the full CMS, however, the L1A signal will be controlled by the Global Muon Trigger.

IV. TEST BEAM ANALYSIS

A. Test Beam Profiles

1. Muon Beams versus Pion Beams

To test the endcap Level-1 Trigger electronics, two beam types were used: muon beams and pion beams, both running at a beam energy of 100 GeV. With the CSCs, the Local Trigger, and the Track-Finder System all designed for muon detection and muon track reconstruction, the muon beam provides a direct method for evaluating the performance of the system. As pions have a mass very similar to that of a muon, a beam of charged pions registers tracks just as a muon beam does.

The muon beam is obtained by inserting an absorber into the beam line, stopping all pions that have not decayed to muons. The spread of the pion beam is noticeably different from the spread of the muon beam. While the pion beam's profile is very focused, with a high intensity along its center path, the profile of the muon beam is much broader with a significantly wider beam spread and long, broad tails, due both in part to the pion absorber in the muon beam path and the resultant angles of the final-state muons from naturally-occurring pion decay. This focused intensity of the pion beam allows the limits of the Level-1 Trigger to be tested, triggering rates at over 20 times the required design capacity. Shown in Figs. 6 and 7, the profiles of each beam are represented in terms of the azimuthal angle (ϕ), here, in half-strip units.

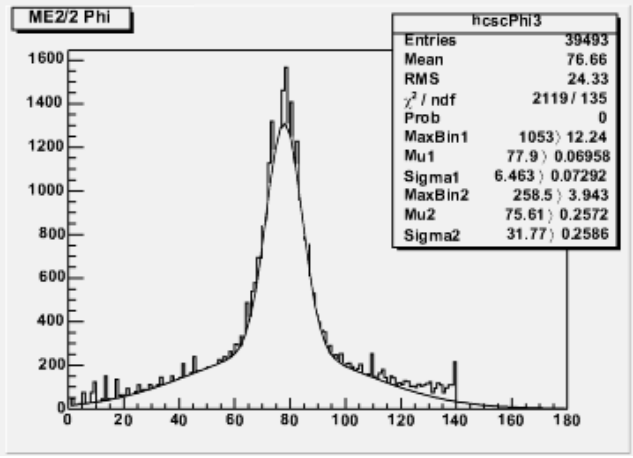

FIGURE 6: Muon beam profile in ϕ

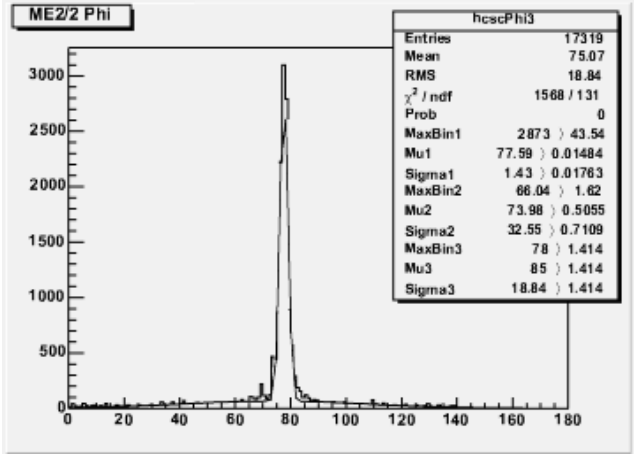

FIGURE 7: Pion beam profile in ϕ

2. Beam Scattering through Iron

Throughout the entire CMS detector, large iron yokes are used for a number of purposes. These iron plates act as mounting support for the CSCs in the endcaps, as an absorption material to minimize the number of non-muons exiting the detector, and, most importantly, as a return for the magnetic flux generated by the superconducting solenoid. The magnetic yoke is divided into the barrel yoke and the endcap yoke (see Fig. 8). Without such a magnetic flux return, the magnetic field generated by the CMS solenoid would be damaging to electronics. Even with the magnetic flux return yokes, the CMS underground control room expects a magnetic field strength of 5 gauss, approximately 10 times the magnetic field strength of the Earth, due to the CMS solenoid. [3] As there will be a significant layer of iron between different stations of the endcap, it was natural to replicate the iron's effect on the beam profile at this summer's beam test.

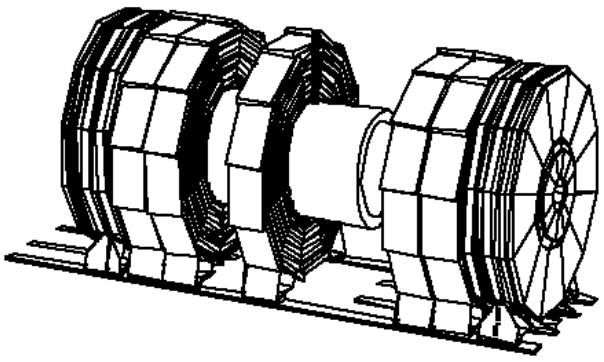

FIGURE 8: The CMS Magnetic Yoke as the five barrel rings and the six endcap

To test the scattering effects of the iron at the CMS Beam Test, a set of iron blocks was assembled to form one large iron block and was placed in the path of the beam. The iron block was approximately half a meter in length (along the path of the beam), with a cross-section of 20 cm by 30 cm. The ability of the iron block to scatter muons is observed by the change in the θ distribution from a run without the iron block to a run with the iron block. Here, θ is the angular diversion (measured in degrees) from the straight-line path of the beam (see Fig. 9) and is calculated by the equation seen in Fig. 10. Note that when converting from half-strip units to mm, the half-strip width varies, due to the trapezoidal shape of the CSC, by wire group position. Here, this was roughly estimated through a linear function of the wire group position, with a range from the minimum half-strip width of ME234/2 to the maximum half-strip width of ME234/2.

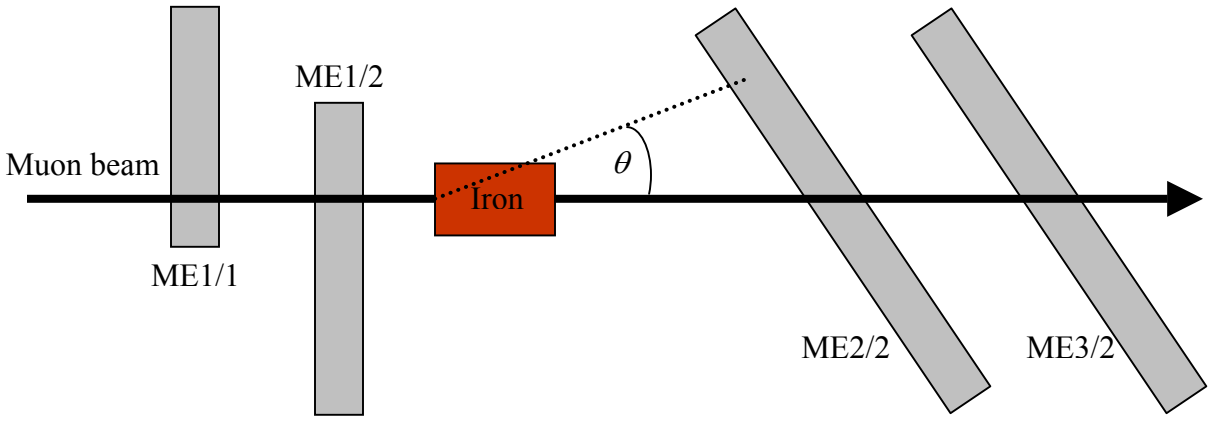

Figure 9: CSC layout for the Beam Test showing θ, the angle of diversion from the normal beam path

$$\theta = \arctan\left(\frac{\Delta\phi}{d}\right), \text{ where:}$$

d is the distance (in mm) from the iron block to chamber ME3/2,
$\Delta\phi$ is the difference in ϕ between ME3/2 and ME2/2
(in mm, as converted by the width of the half-strips)

Figure 10: The equation by which θ is calculated

In comparing two similar runs, it should be noted that, as the majority of the muons travel straight through the iron block, a logarithmic plot is necessary to make the few diverted muons readily visible. The domain of the θ plots was constrained to ±20 half-strips and scaled from the width of a half-strip at the midpoint of an ME234/2 CSC to a θ value of approximately ±8º.

Without Iron:

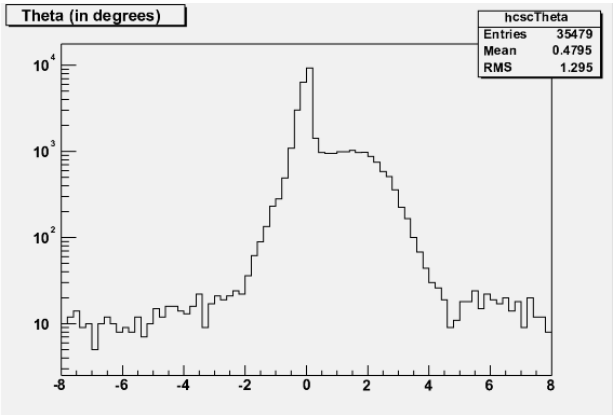

With Iron:

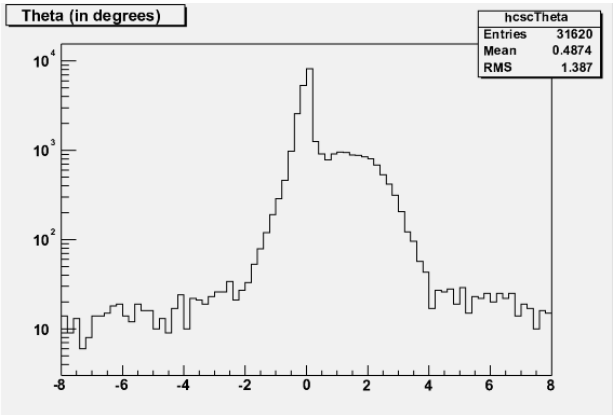

FIGURE 11: Logarithmic plots of θ, measured in degrees, for two runs, one with an iron block in the beam path and one without

Comparing the θ distributions of both runs, it becomes quickly apparent that there is almost no difference between the two. Though the two runs are slightly different in regards to the number of events, the overall distribution did not change significantly. From this, it can be said that the iron block and, in turn, the iron yokes in the CMS detector, have negligible effects on muon beam scattering at a beam energy of 100 GeV. Again, it should be noted the graphs in Fig. 11 are on a logarithmic scale and as such, the vast majority of muons actually pass unobstructed through the iron block.

3. Phi (ϕ) Alignment and Fits

To further explore the beam profile, histogram distributions of ϕ_{local} for the four CSCs were compared. Applying a double-Gaussian fit to the ϕ_{local} distributions allows for a more numerical and less visual evaluation of the distribution shape as seen in Fig. 12.

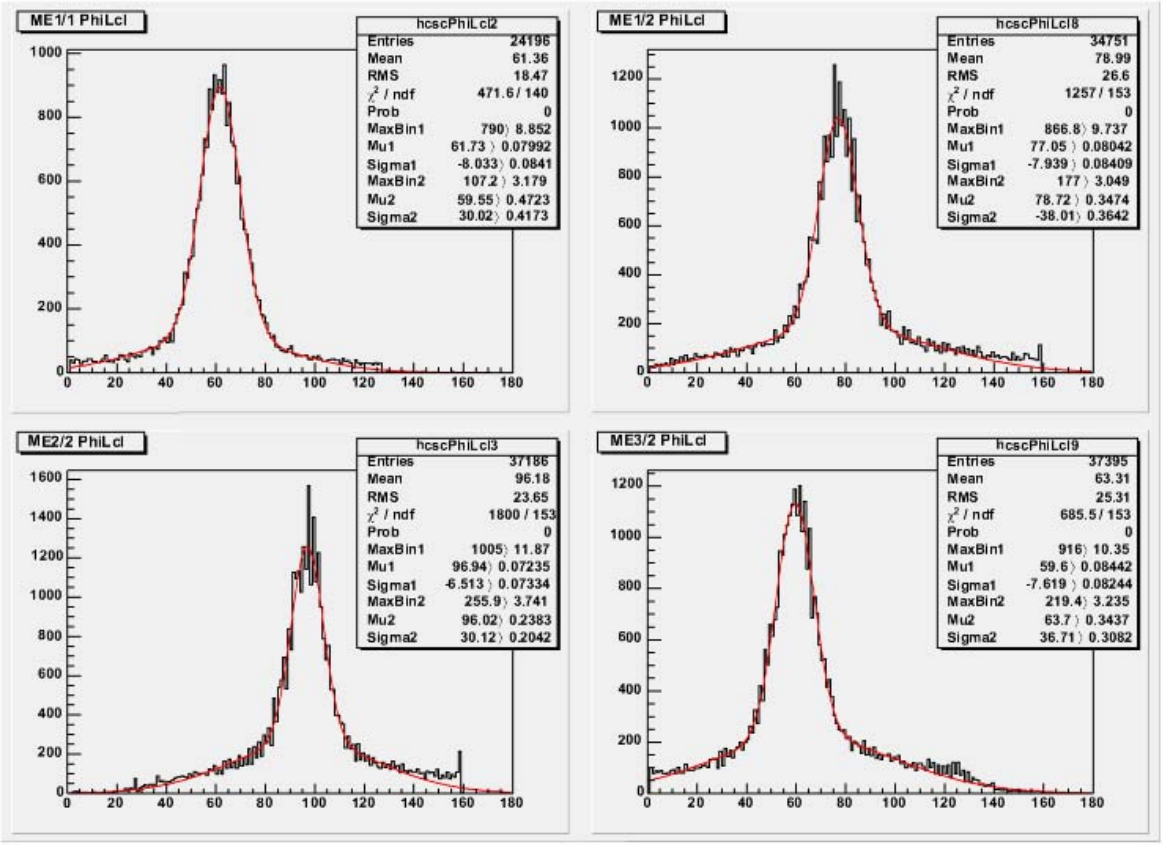

FIGURE 12: The red lines are the fitted double-Gaussians to the ϕ_{local} distributions

The primary purpose of these fits is to provide parameters by which the global ϕ distributions can be normalized for matching peaks. This is especially important to the creation of LUTs specific to a single chamber geometry, such as the linear arrangement of chambers at the beam test, where the peak of the ϕ distribution should all line up. As Fig. 13 shows, after fitting and normalizing the ϕ_{local} distributions, the global ϕ distributions are in fact aligned.

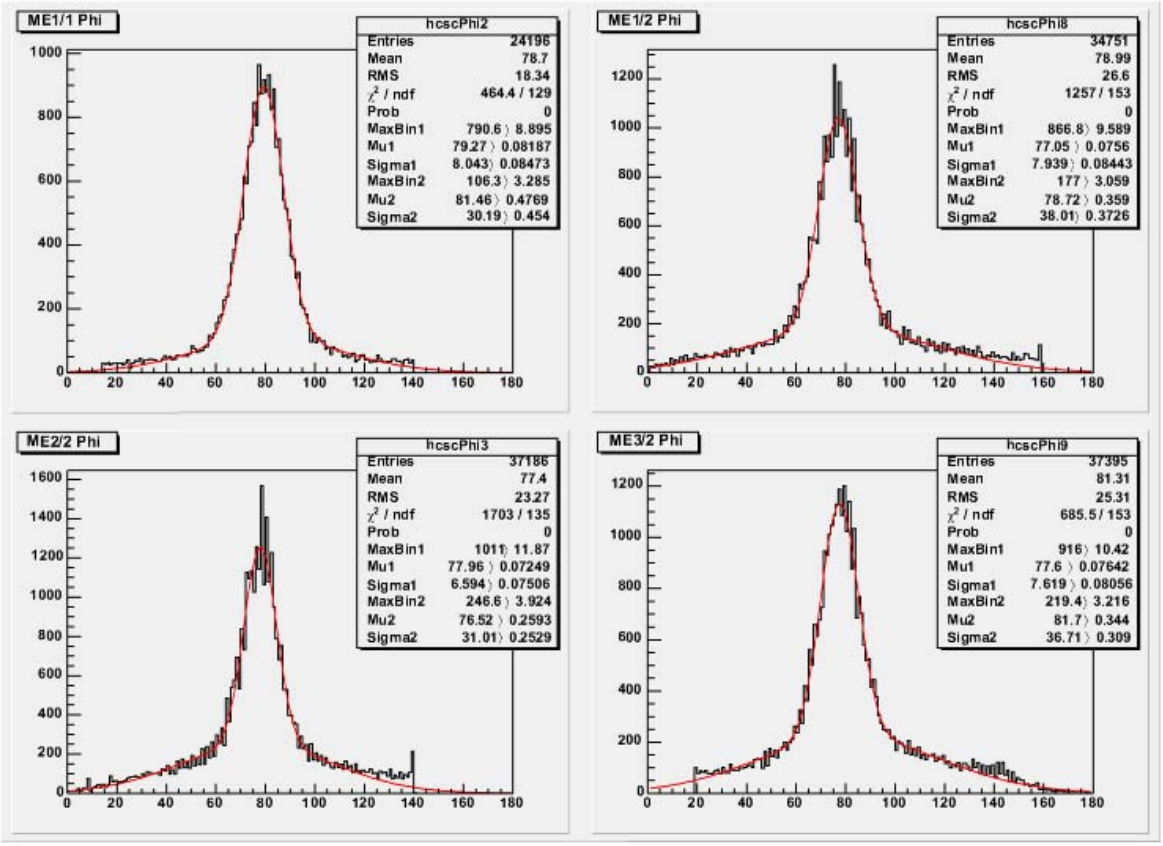

FIGURE 13: The red lines are the fitted double-Gaussians to the global ϕ distributions. Note the near-identical ϕ value for the fitted peak.

B. Sector Processor Core Logic Simulation

The most important aspect of the validation of the Track-Finder's performance lies with the comparison of the SP hardware track output to the software simulation of the Sector Processor Core Logic. The SP Core Logic, written in a modified form of C++, can be implemented as a class within a C++ program or another class. The SP simulation, when properly initialized, will simulate all the processes of the Sector Processor board bit-for-bit, functioning identically to the SP firmware. In addition, the Sector Receiver inputs and the Muon Sorter can also be simulated as part of a larger simulation, mimicking much of the Level-1 Trigger data-chain.

Implementing the Core Logic within a data analysis class did require a number of obstacles to be overcome. Although this implementation of the SP simulation was adapted from another simulation class, slight differences in code structure forced extensive periods of debugging before agreement in results was finally achieved. One surprising realization, however, was the extensive computation time required for the SP simulation, often taking upwards of 4 hours for an average-length run.

In total, the comparison analysis of the SP Core Logic simulation to the hardware track data readout analyzed 83,146 independent events across three separate runs. In all these recorded events, the zero-th muon track output consistently agrees in all output parameters. As can be seen in Fig. 14, a scatter plot comparison of the zero-th muon hardware tracks to the zero-th muon simulation tracks shows a 1-to-1 correlation for the transverse momentum (p_T) of each track. Similarly, Fig. 15 shows a scatter plot comparison of the track mode for the zero-th muon hardware tracks to the zero-th muon simulation tracks run 381. In both scatter

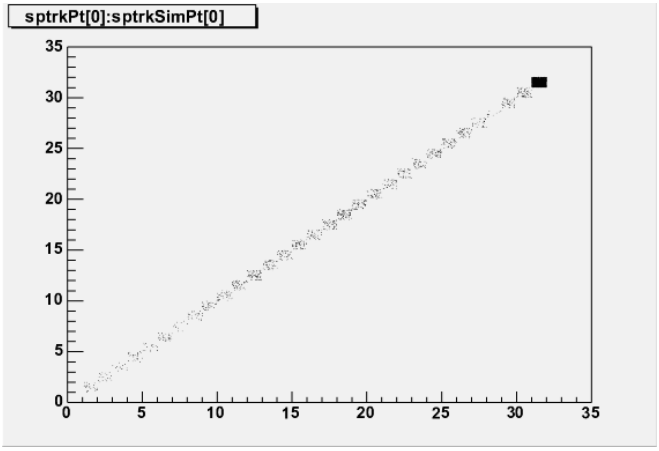

FIGURE 14: A scatter plot comparison of p_T values of the zero-th muon hardware tracks to the zero-th muon simulation tracks in run 379.

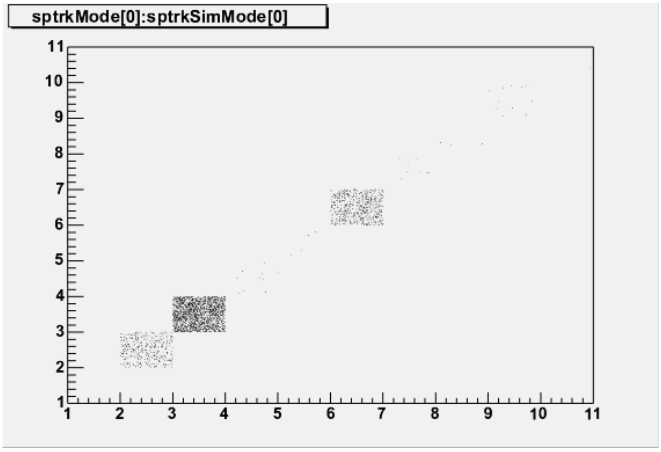

FIGURE 15: A scatter plot comparison of the mode values of the zero-th muon hardware tracks to the zero-th muon simulation tracks in run 381.

plots, each binning area is graphically shown as a shading density corresponding to the number of events found with that specific value.

C. Hardware and Simulation Issues

Not only were there obstacles to be overcome in the implementation of the SP Core Logic simulation, but also there were a number of significant issues that arose from the simulation of the Sector Receiver board and the attempts at optimizing the Track-Finder's performance.

1. Lookup Tables

The accuracy of the transformation of LCT data into the CMS coordinate system relies entirely on the quality of the LUTs. To obtain the full resolution of the CSCs, the LUTs generated by the Object-Oriented Reconstruction for CMS Analysis (ORCA) software must be used. These LUTs, however, are designed for the entire CMS detector and while they may provide a more accurate coordinate system, they are not entirely applicable to a linear arrangement of CSCs, such as the chamber layout of this summer's beam test.

For this reason, specific LUTs, dubbed the 617 set, were generated for use during the 2004 summer beam test. For this 617 set, the Local Phi LUT assigns the half-strip ID of the LCT to the local ϕ value. In the Global Eta LUT, the global η value is assigned from the LCT's wire group number. Finally, to normalize the ϕ distribution, the Global Phi LUT applies an offset value to the local ϕ value, resulting in the global ϕ value.

With the beam test over and all the LCT data stored, it was then proposed that the ORCA Local Phi LUT, which would give a much higher level of ϕ resolution than the half-strip ID, be tested to see what sort of position improvements in ϕ, if any, could be found.

The first sign of a problem can be seen in Fig. 16. Note the large spike at the ϕ value of approximately 125. Here, as in the 617 LUTs, the global ϕ value is calculated from the addition of an offset to the local ϕ value in order for the peaks of the fitted curves (as seen by the red fit lines) to be lined up. Thus, it is safe to deduce that the spike at ~125 actually corresponds to a local ϕ value of zero. Indeed, upon investigation, this was confirmed to be true and the matter of why a spike exists at a local ϕ of zero became the leading question.

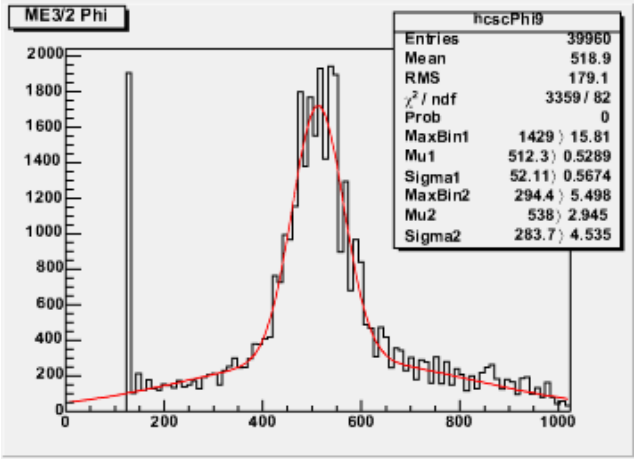

FIGURE 16: The Phi distribution for ME3/2 using the ORCA LUTs

2. Quality Code Issues

As it was soon found, the spike in events having a local ϕ of zero comes from LCTs with a quality value corresponding to a Cathode LCT di-strip pattern. Filling the global ϕ histogram while employing quality exclusions to remove all di-strip muons yields the expected spike-less distribution as seen in Fig. 17.

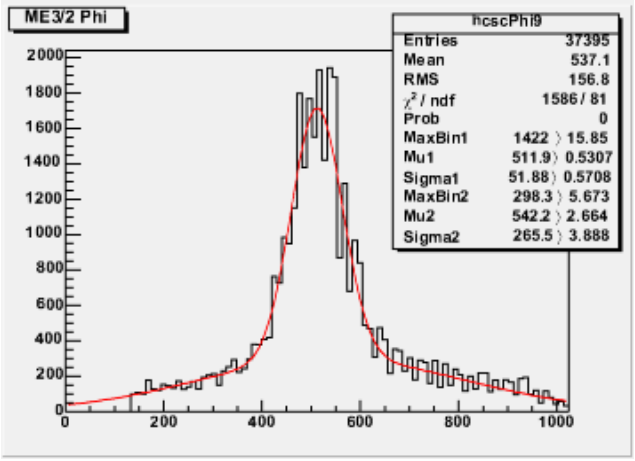

FIGURE 17: The Phi distribution for ME3/2 using the ORCA LUTs and quality exclusions removing all di-strip patters

The problem, however, was found not lie with the di-strip muons themselves, but rather with two conflicting sets of quality code specifications. The current hardware specifications for quality codes contain a range of codes from 1 to 15. On the other hand, the ORCA implementation of quality codes holds a range of 0 to 10. Although, to an extent, one set of

quality codes could be mapped to the other, there is no direct 1-for-1 correlation and there would be, as expected, a loss of information in that transformation. Currently, the hardware quality codes provide a greater level of detail than those of the ORCA simulation and for the full ORCA LUTs to be used, a consensus as to the quality specifications will have to be reached.

3. More Half-strip and Di-strip Issues

The di-strip quality issues notwithstanding, the di-strip muons did, in fact, contribute to a further inaccuracy in measurement. After switching back to the 617 LUT set, it was noted that the strip ID value for di-strip muon tracks was, in fact, only one fourth of the actual value. This is because the di-strips are four times the size of a half-strip and although the strip ID is measured in half-strip units, the di-strip muons report a strip ID corresponding to the di-strip ID. While not a particularly challenging issue, the scaling of the di-strip ID to half-strip units must be addressed for any future LUT creation.

4. Other Anomalies

One peculiar anomaly was first observed when using the ORCA Local Phi LUT. An apparent pattern of alternating high-volume and low-volume histogram bins was observed as in Fig. 18. Each spike is spaced by three, but sometimes four bins, with each low-volume bin being immediately preceded by an even lower-volume bin. While this was originally attributed to be an effect of the ORCA LUT, a similar effect was observed using the 617 LUT set. Although the histogram in Fig. 19 lacks the sharp, single-bin peaks, the same alternating "up and down" pattern can be observed. The detail seen in

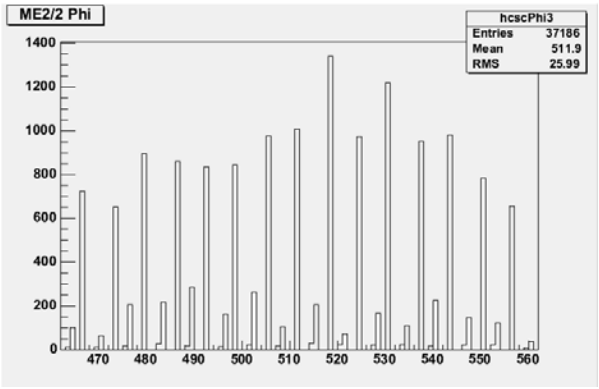

FIGURE 18: Alternating, staggered peaks using ORCA Local Phi LUT

Fig. 18 is most likely due to the increased resolution resulting from the use of the ORCA LUT. For this alternating-peak pattern to be independent of the LUT in use, the cause of this effect would have to have come upstream in the trigger data path, prior to the data's processing in the Sector Receiver.

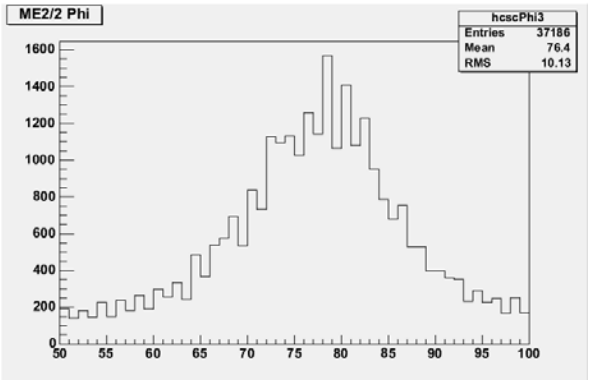

FIGURE 19: Alternating bin volumes found when using the 617 LUT set

V. CONCLUSIONS

The muon beam scattering effects due to the iron block was found to be minimal, if not negligible. This is significant as the tracking of particles in the final CMS detector is desired to be affected by the iron yokes as minimally as possible. Any particle scattering could theoretically impair or at least limit the ability of the Track-Finder to reconstruct muon tracks, depending on the amount of scattering. Further studies of the iron-induced scattering should focus on limiting the muon beam LCTs to only those that pass straight through the iron block in order to remove any scattering effects that occur before the muon beam reaches the iron block.

Most importantly, the perfect agreement between the hardware track output and the software simulation data for all zero-th muon tracks is a significant, although expected, result. As is desired, the Track-Finder should perform exactly as expected, but the intricacy of the design allows the possibility for mistakes in track reconstruction. This external verification that the Track-Finder is indeed performing as expected allows the data output from the Track-Finder to be trusted for its accuracy and validity.

VI. FUTURE DEVELOPMENT

With a week-long beam test coming up in the fall of 2004, a number of preparations can be taken to help reduce the number of problematic issues and improve the speed and quality of data analysis. The ORCA specifications for LCT quality must be redesigned to match the hardware quality specifications. This will allow a reconstruction of the ORCA LUTs, of which the Local Phi LUT can be used at beam tests to increase the accuracy and detail of track-finding. Also, a remapping of di-strip pattern muons to the proper half-strip units is necessary for proper LUT creation and data analysis. With effective LUTs, current software can be used to automatically fit and normalize histogram distributions for fast data analysis.

In addition, a third-generation and final production Track-Finder is currently under development. Although it is not a significant update from the SP2002 board, this updated Track-Finder will require extensive testing to ensure, as was done for the SP2002 Track-Finder, that the board is operating as designed and without error. An accurate, working Track-Finder is essential to the performance of the Level-1 Trigger and so similar simulation and analysis will be necessary for future studies.

REFERENCES

[1] *CMS: The Muon Project Technical Design Report*, CERN/LHCC 97-32. CMS TDR 3, 15 December 1997.

[2] *CMS: The Trigger and Data Acquisition project, Volume I. The Level-1 Trigger Technical Design Report*, CERN/LHCC 2000-38. CMS TDR 6.1, 15 December 2000.

[3] *CMS: The Magnet Project Technical Design Report*, CERN/LHCC 97-10. CMS TDR 1, 2 May 1997.

ACKNOWLEDGEMENTS

Nicholas S. Park would like to thank his mentor and co-author Dr. Darin Acosta for providing this and other research opportunities. He would also like to thank Dr. Holger Stoeck, Bobby Scurlock, and Lindsey Gray for their support in this project. In addition, he offers much thanks to UF REU Program Director Kevin Ingersent, Associate Director Alan Dorsey, Program Assistant Donna Balkcom, and Graduate Assistant Wayne Bomstad for their leadership, direction, and support of the University of Florida Summer 2004 Research Experiences for Undergraduates Program. Furthermore, the accommodations provided by the University of Florida Department of Physics are greatly appreciated.

This project was completed with the financial support of the National Science Foundation's Research Experiences for Undergraduates Program, through grants DMR-9820518 and DMR-0139579.